AGU PUBLICATIONS

JGR

Journal of Geophysical Research: Space Physics

RESEARCH ARTICLE
10.1002/2017JA024623

**Key Points:**
- A superposed epoch method together with background maps are used to evaluate ionospheric perturbations
- Ionospheric perturbations occur 5 days before earthquakes of magnitude >5
- A postseismic effect is observed just after the earthquakes as it is expected

**Correspondence to:**
M. Parrot,
mparrot@cnrs-orleans.fr

**Citation:**
Yan, R., Parrot, M. & Pinçon, J.-L. (2017). Statistical study on variations of the ionospheric ion density observed by DEMETER and related to seismic activities. *Journal of Geophysical Research: Space Physics*, *122*, 12,421–12,429. https://doi.org/10.1002/2017JA024623

Received 27 JUL 2017
Accepted 18 NOV 2017
Accepted article online 27 NOV 2017
Published online 7 DEC 2017



# Statistical Study on Variations of the Ionospheric Ion Density Observed by DEMETER and Related to Seismic Activities

**Rui Yan[1,2], Michel Parrot[1], and Jean-Louis Pinçon[1]**

[1]University of Orléans, LPC2E/CNRS, Orléans, France, [2]Institute of Crustal Dynamics, China Earthquake Administration, Beijing, China

**Abstract** In this paper, we present the result of a statistical study performed on the ionospheric ion density variations above areas of seismic activity. The ion density was observed by the low altitude satellite DEMETER between 2004 and 2010. In the statistical analysis a superposed epoch method is used where the observed ionospheric ion density close to the epicenters both in space and in time is compared to background values recorded at the same location and in the same conditions. Data associated with aftershocks have been carefully removed from the database to prevent spurious effects on the statistics. It is shown that, during nighttime, anomalous ionospheric perturbations related to earthquakes with magnitudes larger than 5 are evidenced. At the time of these perturbations the background ion fluctuation departs from a normal distribution. They occur up to 200 km from the epicenters and mainly 5 days before the earthquakes. As expected, an ion density perturbation occurring just after the earthquakes and close to the epicenters is also evidenced.

## 1. Introduction

This paper deals with a statistical analysis of the ionospheric ion density observed by the satellite DEMETER above areas of seismicity. DEMETER was a quasi-polar low altitude satellite (660 km) in operation between 2004 and 2010 with a nearly Sun synchronous orbit (10.30 and 22.30 LT) and equipped with a payload to measure ionospheric waves and densities (Parrot, 2006).

In the past, some statistics have already been done with different ionospheric parameters. Variations have been observed a few days before the earthquakes. Hayakawa et al. (2010) have reported on the statistical correlation, based on their VLF measurements during 7 years, of lower ionospheric perturbations with earthquakes with magnitude (*M*) larger than 6 and with shallow depth. Then the first attempt on the statistical association of ionospheric electron density perturbations with earthquakes was done on the basis of a rather long database by the satellite Intercosmos 24 (Afonin et al., 1999). Liu et al. (2004) performed a statistical analysis of global ionosphere map (GIM) total electron content (TEC) during the 20 earthquakes with *M* larger than or equal to 6.0 in Taiwan from September 1999 to December 2002. Later on, using the same parameter, they have shown that the GIM TEC above the epicenter decreases 3–5 days before 17 earthquakes with *M* larger than or equal to 6.3 during the 10 year period from 1 May 1998 to 30 April 2008 (Liu et al., 2009). Using TEC data recorded in Japan, a superposed epoch analysis has been done by Kon, Nishihashi, and Hattori (2011) to check anomalies associated with earthquakes with *M* larger than or equal to 6.0 during 12 years (1998–2010). Their statistical results indicate that positive TEC anomalies can be observed from 1 up to 5 days before earthquakes at a distance up to 1,000 km from the epicenters.

Statistical analyses have been also done with the DEMETER data during many earthquakes. A statistical study on the variations of the electric field up to 10 kHz has been performed (Němec et al., 2008; Němec, Santolík, & Parrot, 2009). About 2,000 earthquakes with *M* larger than or equal to 4.8 have been taken into account. This study has shown that, during the night, there is a statistically significant decrease of the wave intensity several hours before earthquakes. The results of Němec et al. (2008, 2009) were confirmed by Píša et al. (2012, 2013) using the complete DEMETER data set at the end of the mission (9,000 earthquakes). In fact, the decrease of the wave intensity occurs close to a frequency (1.7 kHz) during the nighttime. This frequency is inversely proportional to the height of the Earth-ionosphere waveguide. The cutoff frequency is found to be increasing, so that the height of the ionosphere is statistically lower above epicenters. These studies show statistically that there may be an excess of ionization at the bottom of the

ionosphere above epicenters of future earthquakes. This satellite result is likely to be consistent with the VLF finding by Hayakawa et al. (2010). Another statistical study of ionospheric perturbations in relation with equatorial anomalies observed by DEMETER has been done by Hobara et al. (2013) using the electric field measurement, who have shown a weak correlation between nighttime ionospheric perturbations and land earthquakes. A similar work by Ryu et al. (2014) investigated the correlation between seismic activity and equatorial plasma density variations. They indicate that equatorial ionization anomaly (EIA) enhancements can be correlated with earthquakes of large magnitude ($M > 5.0$), which seems to support the early work by Molchanov et al. (2002).

Other statistical analyses have been performed with the DEMETER density data recorded at the altitude of the satellite. Using a superposed epoch method, He et al. (2011) have compared the electron density close to epicenters between and 1 and 30 days before the earthquakes with the electron density recorded at the same location between 31 and 75 days before. They have statistically demonstrated that there is an increase of the electron density close to the epicenters during nighttime. This increase depends on $M$ and on the depth of the earthquakes. Statistical analyses have been performed using the automatically determined ion density peaks in the complete DEMETER data set (6.5 years) (Li & Parrot, 2012, 2013; Parrot, 2011, 2012). The occurrence of the peaks (time and position) is then compared to the occurrence of earthquakes. They have shown that the number of good fits increases with the earthquake magnitude and that the number of perturbations is higher on the day of the earthquakes, and then slowly decreases on the days after them.

The mechanisms to explain these ionospheric perturbations are described and discussed with Lithosphere-Atmosphere-Ionosphere Coupling (LAIC) models by Hayakawa and Molchanov (2004), Pulinets (2009), Freund (2011), Pulinets et al. (2015), and De Santis et al. (2015). The ionospheric density variations can be triggered by change of the electric field and the current in the global electric circuit between the bottom of the ionosphere and the Earth's surface where electric charges associated with the stressed rocks can appear (Kelley, Swartz, & Heki, 2017; Kuo et al., 2011). Other hypotheses and modeling can be found in monographs (Hayakawa, 2009, 2012; Hayakawa, 2015; Sorokin, Chmyrev, & Hayakawa, 2015), in reviews by Pulinets (2009, 2012), Pulinets and Ouzounov (2011), and references therein. At the same time, gas release before earthquakes (Baragiola, Dukes, & Hedges, 2011; Harrison, Aplin, & Rycroft, 2010; Omori et al., 2007; Pulinets, 2007; Sorokin, 2007) and atmospheric heating, which can be observed with infrared experiments onboard satellites (Ouzounov et al., 2007, 2011), have been considered. Furthermore, atmospheric gravity wave is also a possible candidate for the LAIC (Molchanov & Hayakawa, 2008).

The work presented in this paper has some similarity with the study of He et al. (2011). But in our study, the ion density is used instead of the electron density, the method to compare the density at the time of the earthquakes with the background density is different. Besides the distance occurrence of the perturbations, there is a study about their time occurrence, and the problem of aftershocks is carefully considered. Section 2 is related to the data: (i) the ion density given by the experiment IAP onboard DEMETER and (ii) the earthquakes. The statistical method is described in section 3. Section 4 presents the results with all events occurring during the DEMETER mission between 2005 and 2010. They are discussed in section 5. Finally, section 6 presents some conclusions.

## 2. The Data

### 2.1. The IAP Data Used for This Study

The details of the IAP experiment can be found in Berthelier et al. (2006). Only nighttime data are used because detection of ionospheric perturbations related to earthquakes is not expected during daytime when the density variation is strongly dominated by the Sun. The data are selected from 2005 to 2010. Data recorded during 2004 are not considered here for the following two reasons: (i) the solar activity was very active during 2004, and (ii) the satellite was often either in commissioning phase or safe mode. The IAP instrument was operated in two scientific modes (burst and survey) with different time resolution. For this study, the burst mode data are averaged to have the same time resolution as in the survey mode (4 s). With information about the orbitography and the magnetic activity, an ionospheric ion density database is built where each record contains the date, the time, the latitude, the longitude, the densities of the main ions ($H^+$, $He^+$, and $O^+$), the total ion density (obtained by adding the contributions of $H^+$, $He^+$, and $O^+$), the ion temperature, the half-orbit number, and a $K_p$ value. The $K_p$ values in the

database are the ones for which the difference between the half-orbit end time and the $K_p$ time is minimum. In this paper we restricted our analysis to data with $K_p$ smaller than or equal to 3 to avoid density perturbations due to magnetic activity.

### 2.2. The List of Earthquakes

The considered earthquake database includes 20,547 earthquakes occurring from 2005 to 2010, with $M$ larger than or equal to 4.8 (U.S. Geological Survey: http://www.usgs.gov), which are listed in chronological order. The parameters present in the list are the date, the time, the position (latitude and longitude), the magnitude ($M$), and the depth.

It is well known that an ionospheric perturbation is generated right after the shock due to the propagation of an acoustic-gravity wave (see for example, Astafyeva et al., 2013, and references therein). This aftershock effect can severely alter the meaning of the statistic study performed in the frame of this study. Accordingly, before performing the statistical analysis, we have preprocessed the data to carefully remove both the aftershocks in the list of earthquakes and the corresponding data in the database. Practically, this is done by associating an area of $2° \times 2°$ centered on the epicenter of all earthquakes in the list. The list is then processed in chronological order as follows: for a given earthquake, characterized by its occurrence time and its associated area, any other earthquake occurring inside the area up to less than 15 days after the occurrence time is systematically removed from the list and the corresponding IAP data removed from the database. Fifteen days is the largest time period where anomalies before earthquakes are considered in the frame of our statistical study (see next section for more details about this point). Moreover, if aftershocks occurred during the 15 day interval, data corresponding to the days of the aftershocks are removed. After this preprocessing 10,320 earthquakes are remaining in the list.

## 3. The Statistical Method

### 3.1. The Background Maps

To determine whether or not an anomalous ion density perturbation is occurring at the time of the earthquakes and to quantify this perturbation, it is necessary to compare it to the ion density variation expected in case of no seismic activity. To achieve this task we have built background maps including this information. First, the Earth's map is divided into cells with $\Delta\text{Lat} = 2°$ and $\Delta\text{Long} = 4°$. Then, for each cell, an average value $\overline{x}$ of the ion density data and its corresponding variance $\sigma$ are calculated using all the available data with $K_p \leq 3$ as a function of the position around the Earth and by averaging data over a given time. The integration time to calculate $\overline{x}$ and $\sigma$ must be carefully selected because the ion density varies not only as a function of the seasons but also as a function of the years due to the fact that our period of investigation corresponds to the declining phase of the nontypical solar cycle 23 (Lühr & Xiong, 2010). To take into account the density variation as a function of time (seasons and years), solstices, equinoxes, winter, and summer are all considered. In order to ensure that the obtained background maps are statistically significant, several months of data are used to generate a single map. One must notice that the background maps include data that are recorded above seismic zones as we do not know a priori the area that could be affected by each earthquake and the time period when a precursor could occur.

To give an example concerning the period November 2006 to February 2008, four background maps have been built as follows: (i) November–December 2006 and January–February 2007, (ii) March–April 2007 and September–October 2007, (iii) May-June-July-August 2007, and (iv) November–December 2007 and January–February 2008. In total, for the period 2005–2010, 19 background maps have been generated. Examples of background maps showing the averaged ion density are given in Figure 1. The top panel and the middle panel of Figure 1 display background maps calculated using the same months but for years 2005 and 2007, respectively. Their comparison shows a significant decrease of the averaged ion density between these two years. Similarly the comparison of background maps displayed in the middle and bottom panels of Figure 1 shows the important difference between the seasons in 2007 as it is usual.

### 3.2. Characterization of Ion Density Fluctuations Above Seismic Areas

As mentioned in section 3.1, we would like to compare the data related to earthquakes with those in the background maps to evidence a possible ion density variation associated with seismic activity. To select

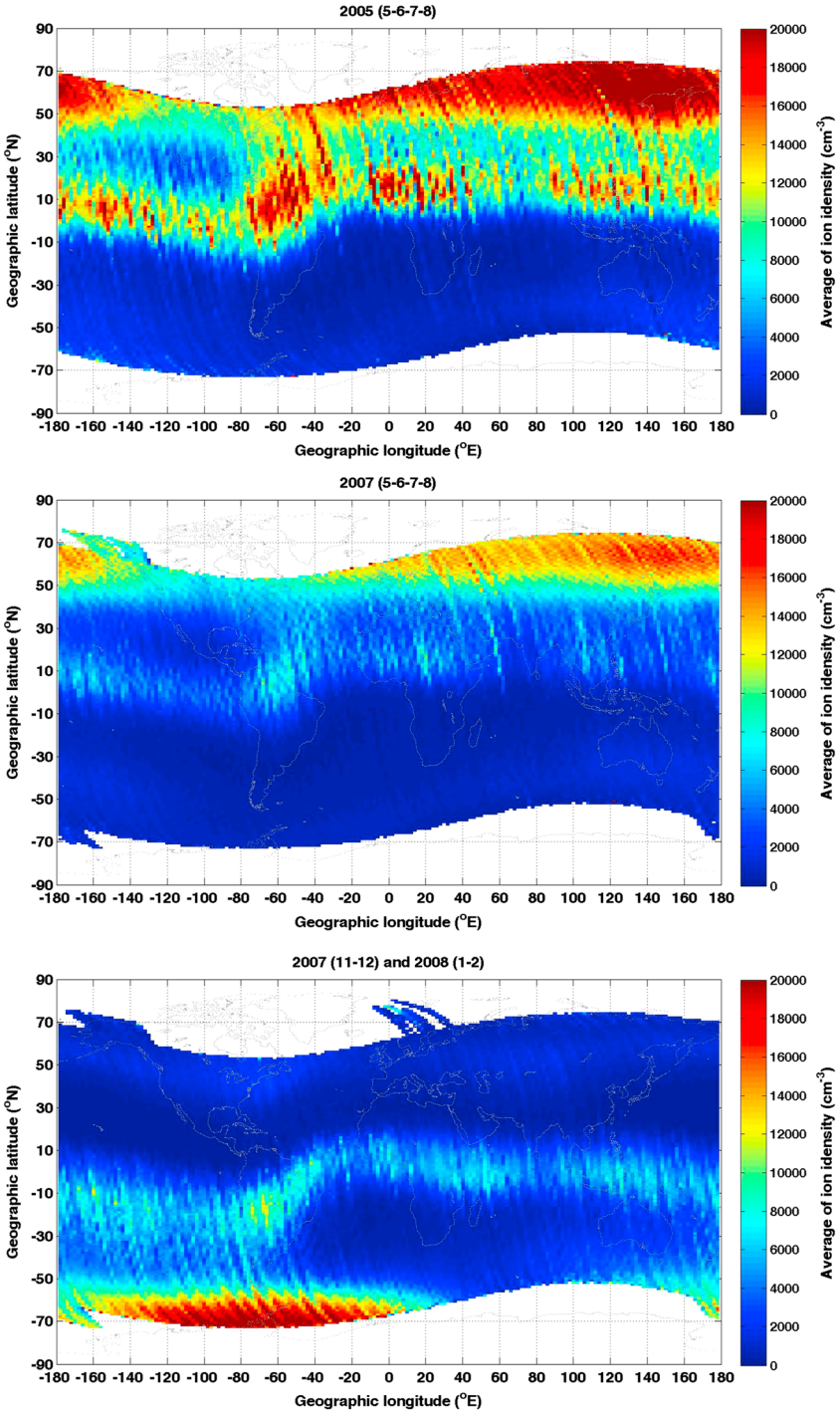


**Figure 1.** Examples of background maps: (top) May-June-July-August 2005, (middle) May-June-July-August 2007, and (bottom) November–December 2007 and January–February 2008.

the earthquake related data we first need to define the time interval and the space area of interest for our study. The time interval of interest was arbitrarily fixed to be from 15 days before the occurrence time of earthquakes and until 5 days after. The space area of interest was taken as a disk with radius of 1,000 km centered on the epicenter of earthquakes. Each ion density value $N_i$ of the ionospheric ion density database that is both inside the time interval and space area associated with an earthquake is considered. Taking into account both the time and the location of the measurement, each $N_i$ can be related to one unique cell of a unique background map (see Figure 2). Each data point is normalized

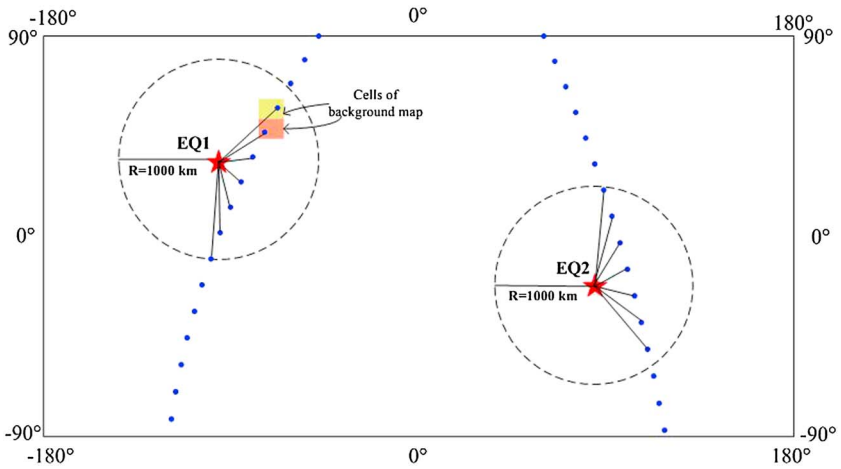


**Figure 2.** Sketch map showing the data point on the orbit (blue dots), earthquake epicenters (red star), and the areas around epicenters (dashed circles) that are considered to select earthquake related data. The radius of the circles is not at the scale of the map.

considering the average and the standard deviation values in the corresponding cell of the background map. Then, for the earthquake $j$, the new calculated quantity $(D_i)_j$ is given by

$$(D_i(\Delta l, \Delta t))_j = \frac{(N_i(\Delta l, \Delta t))_j - \overline{x}_j}{\sigma_j} \quad (1)$$

$(D_i)_j$ is a function of the distance ($\Delta l$) between the location where the data are measured projected on the Earth's surface and the epicenter of the considered earthquake $j$ and function of the time difference ($\Delta t$) between the measurement time of the data and the occurrence time of the earthquake $j$. If earthquakes would have no effects on the ionospheric ion density, then the statistics of $N_i$ should be similar to the statistics of the ion density measurements used to build the background maps and, in such a case, the averaged $(D_i)_j$ distribution should be Gaussian like. The histogram of the $(D_i)_j$ values obtained when all earthquakes are considered is presented in Figure 3. This distribution is very asymmetric, which strongly suggests a very different behavior depending on whether we are considering positive or negative $(D_i)_j$. For negative $(D_i)_j$, noted hereafter $(D_i^-)_j$, the distribution is roughly Gaussian, whereas for positive $(D_i)_j$, noted $(D_i^+)_j$, the distribution is obviously not Gaussian.

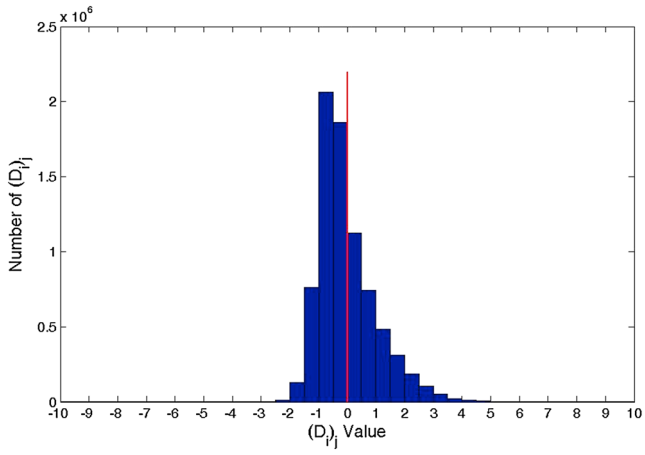


**Figure 3.** The histogram of the $(D_i)_j$ values obtained when all earthquakes are considered.

Some LAIC models suggest that the ionospheric effect can be positive or negative. It can be explained by either positive or negative direction of anomalous electric field on the ground surface (Pulinets, 2009). Regarding the ion density measurements performed onboard DEMETER, the obtained $(D_i)_j$ distribution is clearly in favor of an anomalous statistical increase in the ionospheric ion density above earthquakes. The asymmetry of the $(D_i)_j$ distribution and the lack of features for the $(D_i^-)_j$ distribution are the reasons justifying the approach adopted in this paper where positive and negative $(D_i)_j$ are studied separately with a focus on the $D_i^+$ distribution.

### 3.3. The Superposed Epoch Method

The superposed epoch method is a statistical method to highlight a weak but a significant signal from noisy data. This technique can reveal typical characteristics, precursors, time schedules, periodicities, and consequences of a special event (see for example Adams, Mann, & Ammann, 2003; Hayakawa et al., 2010; Hocke, 2008; Kon et al., 2011). In our superposed epoch method a grid is considered where the horizontal axis is

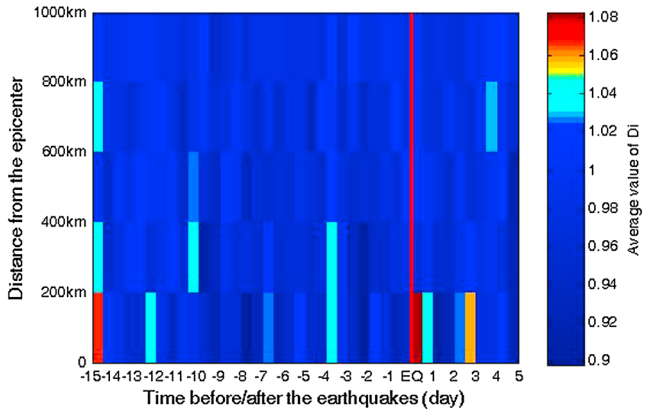


**Figure 4.** Grid showing the result of the superposed epoch method as a function of distance from the epicenters and as a function of the difference between the time of the data registration along the orbits and the occurrence time of the earthquakes. The vertical red line corresponds to the occurrence time of the 10,320 earthquakes with $M \geq 4.8$ considered in this study. The dimension of a cell is 200 km × 12 h. The value inside each cell corresponds to the average value of $D_i^+$ and is coded according to the color scale on the right. This color scale is adapted to emphasize the variation of $D_i^+$ (see text).

related to time (before/after earthquakes) and the vertical axis to the distance from earthquake epicenters. It is assumed that all earthquake epicenters have the same location (distance = 0) and all earthquakes occur at the time equal to 0. For each earthquake the data are cumulated in appropriate cells. It means that all $D_i$ values are allocated to cells that are a function of the distance from the epicenters and a function of the time before/after the earthquakes (see Figure 4). The time interval is ranging from 15 days before to 5 days after the earthquakes, and the epicenter distance is ranging from 0 up to 1,000 km. In this grid, each cell has a dimension of 200 km × 12 h. Finally, taking into account all earthquakes an average value $D_i^{+/-}$ of all positive $(D_i^+)_j$ or negative $(D_i^-)_j$ values is calculated. The $D_i^+$ in each cell of the grid is plotted in Figures 4 and 5 according to the color scale on the right. The obtained $D_i^+$ values are ranging from 0.898 to 1.0827 (Figure 4), whereas the $D_i^-$ values are ranging from −0.7058 to −0.6217. If we select earthquakes with magnitude greater than 5 (Figure 5), then $D_i^+$ is now ranging from 0.8283 to 1.1434, whereas $D_i^-$ is ranging from −0.73 to −0.5953.

Assuming that the background ion fluctuations are following a Gaussian distribution characterized by an average value $\overline{x}$, and a standard deviation $\sigma$, we can estimate the value of $D_i^+$ if the earthquakes have no effects on the ionospherioc ion density. In such a case $D_i^{+/-}$ is then defined as

$$D_i^{+/-} = \frac{\left\langle N_i^{+/-} \right\rangle - \overline{x}}{\sigma} \tag{2}$$

where $\left\langle N_i^+ \right\rangle$ ($\left\langle N_i^- \right\rangle$) has to be calculated considering only ion density values larger (smaller) than the averaged background ion density. Using a Gaussian distribution $\left\langle N_i^+ \right\rangle$ can be estimated as

$$\left\langle N_i^+ \right\rangle = \frac{2}{\sqrt{2\pi}\sigma} \int_{\overline{x}}^{\infty} x\, e^{\frac{-(x-\overline{x})^2}{2\sigma^2}} dx = \overline{x} + \sigma\sqrt{2/\pi} \tag{3}$$

Consequently, if the $N_i^+$ values behave just like background fluctuations, we should have using equations (2) and (3) $D_i^+ \approx 0.8$. Similarly, we should have $D_i^- \approx -0.8$.

The comparison with the experimental $D_i$ distribution (Figure 3) leads to the following conclusions: First, the $D_i^-$ distribution is Gaussian like, it has an average value close to −0.7 not too far from the theoretical result in case of no effects from the earthquakes, and presents small fluctuations around the average value. Second, the $D_i^+$ distribution is not Gaussian, with an average value close to 1 and fluctuations around the average twice larger than for the negative $D_i$. The significant departure of $D_i^+$ with respect to the Gaussian situation is of special interest for our study, and the main features of this distribution are discussed in the next section.

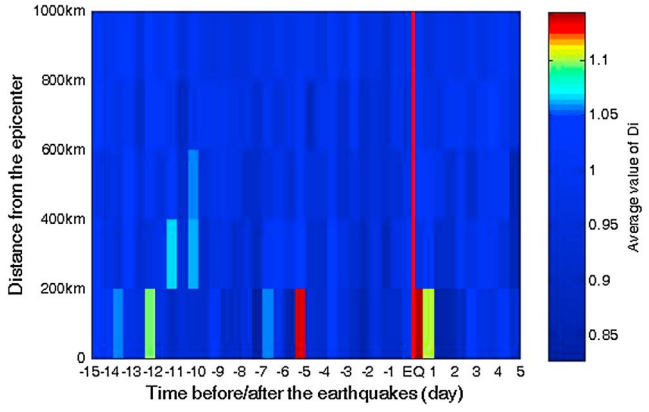


**Figure 5.** Same as in Figure 4 but for earthquakes with magnitude >5 (5,426 earthquakes).

## 4. The Results

Figure 4 represents the final result of the statistical analysis when all earthquakes with $M$ larger than or equal to 4.8 are considered. In Figure 4 a density perturbation is observed close to the epicenters (less than 200 km) and just after the earthquakes.

More interesting results are obtained when earthquakes with larger $M$ are considered. Figure 5 is the result related to earthquakes with $M$ larger than 5. The appearance of the anomaly just after the earthquakes remains as it is in Figure 4 but with a significant intensity. The more important fact is that another perturbation is observed mainly 5 days before the earthquakes at less than 200 km from the epicenters with a value that can reach 1.15. This quantity is statistically significant because it corresponds to the

average of 2,048 $D_i$ values related to 185 different earthquakes. It can be shown that these 185 earthquakes do not have a particular location.

## 5. Discussions

It is generally accepted that the radius of seismic area where changes can be expected is given by the Dobrovolsky's formula

$$R = 10^{0.43M} \tag{4}$$

where $R$ is the radius of the earthquake preparation zone in kilometers and $M$ is the earthquake magnitude (Dobrovolsky, Zubkov, & Myachkin, 1979). For $M$ equal to 5, $R$ is equal to 141 km, which is in relatively good agreement with the results of our analysis. We must consider that an average value of the earthquake magnitudes in our statistical study is close to 5 because the number of earthquakes decreases a lot with an increase in $M$. Then it is likely that ionospheric observations are mainly observed up to 200 km (the dimension of our cell).

The time occurrence of the ionospheric perturbations before the earthquakes is a little bit different from the previous works mentioned in section 1 because those anomalies were mainly observed just before the earthquakes (−1 to −5 days). In our case it is mainly at −5 days, and there is really a gap just before the earthquakes where no anomaly is observed. This can be due to the fact that the previous analyses were done at different locations in the ionosphere by sounders or using the TEC, which is an integrated parameter. However, Ryu et al. (2014) have shown that EIA was enhanced from approximately 2 weeks before to a few days after the occurrence of very large earthquakes.

The distance occurrence of the ionospheric perturbations before earthquakes is consistent with the statistical study by He et al. (2011). In their analysis, the result shows that there are anomalies close to the epicenters prior to the occurrence of earthquakes. When the distance increases, the intensity of the perturbations decreases.

A very interesting point that consolidates the validity of our results is that an effect is observed just after the occurrence of the earthquakes. The earthquakes can be compared to explosions, and it is well known that the induced acoustic gravity waves or the tsunamis that could occur for earthquakes below the sea can perturb the ionosphere (see, for example, Rolland et al., 2011, and references therein). One cannot also rule out the hypothesis that processes occurring during the preparatory phase of the earthquakes are valid even after the shock when the Earth's crust returns to equilibrium along the fault.

## 6. Conclusions

A statistical analysis has been done with the ion density recorded by the low-altitude satellite DEMETER during several years to check if there are ionospheric perturbations prior to earthquakes. The ion density registered at the time of earthquakes was compared to that averaged over a long time period. To take into account all earthquakes a superposed epoch method was considered, and the following results based on nighttime data have emerged:

1. Some significant ionospheric anomalies where the ion density distribution differs from a normal distribution can be observed 5 days before earthquakes with $M$ larger than 5 at distances up to 200 km from their epicenters;
2. A postseismic effect is observed in the ionosphere after the earthquakes.

The observed perturbations are real but can be evidenced only statistically. Consequently, ionospheric ion density measurements alone cannot be used for earthquake forecasting, but an earthquake warning based on this study might be plausible.

**Acknowledgments**
This work is supported by the National Natural Science Foundation of China (41404058), the civil aerospace research project "The research and development on ground verification technology of CSES data," and special fund for public welfare of Scientific Research Project of ICD, CEA (ZDJ201411). The authors thank ISSI-BJ for the support of our international team working on "Validation of Lithosphere-Atmosphere-Ionosphere-Magnetosphere Coupling (LAIMC) as a Concept for Geospheres Interaction by Utilizing Space-Borne Multi-Instrument Observations". This work is mainly related to data recorded by the ion spectrometer IAP of the microsatellite DEMETER that was operated by the French Centre National d'Etudes Spatiales (CNES). The authors thank J.J. Berthelier, the PI of IAP for the use of the data. The DEMETER data shown in this paper can be obtained at https://cdpp-archive.cnes.fr/. The earthquakes can be obtained at http://www.usgs.gov.

## References

Adams, J. B., Mann, M. E., & Ammann, C. M. (2003). Proxy evidence for an El Niño-like response to volcanic forcing. *Nature*, *426*(6964), 274–278. https://doi.org/10.1038/nature02101

Afonin, V. V., Molchanov, O. A., Kodama, T., Hayakawa, M., & Akentieva, O. A. (1999). Statistical study of ionospheric plasma response to seismic activity: Search for reliable result from satellite observations. In M. Hayakawa (Ed.), *Atmospheric and ionospheric electromagnetic phenomena associated with earthquakes* (pp. 597–617). Tokyo, Japan: Terra Scientific Publishing Company.

Astafyeva, E., Shalimov, S., Olshanskaya, E., & Lognonné, P. (2013). Ionospheric response to earthquakes of different magnitudes: Larger quakes perturb the ionosphere stronger and longer. *Geophysical Research Letters*, *40*, 1675–1681. https://doi.org/10.1002/grl.50398

Baragiola, R. A., Dukes, C. A., & Hedges, D. (2011). Ozone generation by rock fracture: Earthquake early warning? *Applied Physics Letters*, *99*(20), 204101. https://doi.org/10.1063/1.3660763

Berthelier, J. J., Godefroy, M., Leblanc, F., Seran, E., Peschard, D., Gilbert, P., & Artru, J. (2006). IAP, the thermal plasma analyzer on DEMETER. *Planetary and Space Science*, *54*(5), 487–501. https://doi.org/10.1016/j.pss.2005.10.018

De Santis, A., De Franceschi, G., Spogli, L., Perrone, L., Alfonsi, L., Qamili, E., … Tao, D. (2015). Geospace perturbations induced by the Earth: The state of the art and future trends. *Physics and Chemistry of the Earth*, *85-86*, 17–33. https://doi.org/10.1016/j.pce.2015.05.004

Dobrovolsky, I. R., Zubkov, S. I., & Myachkin, V. I. (1979). Estimation of the size of earthquake preparation zones. *Pure and Applied Geophysics*, *117*(5), 1025–1044. https://doi.org/10.1007/BF00876083

Freund, F. (2011). Pre-earthquake signals: Underlying physical processes. *Journal of Asian Earth Sciences*, *41*(4-5), 383–400. https://doi.org/10.1016/j.jseaes.2010.03.009

Harrison, R. G., Aplin, K. L., & Rycroft, M. J. (2010). Atmospheric electricity coupling between earthquake regions and the ionosphere. *Journal of Atmospheric and Solar - Terrestrial Physics*, *72*(5-6), 376–381. https://doi.org/10.1016/j.jastp.2009.12.004

Hayakawa, M. (2009). *Electromagnetic phenomena associated with earthquakes* (1st ed., 279 pp.). Kerala, India: Transworld Research Network.

Hayakawa, M. (Ed.) (2012). *The frontier of Earthquake prediction studies* (1st ed., 794 pp.). Japan: Nihon-Senmontosho-Shuppan.

Hayakawa, M. (2015). *Earthquake prediction with radio techniques* (1st ed., 294 pp.). Singapore: John Wiley. https://doi.org/10.1002/9781118770368

Hayakawa, M., Kasahara, Y., Nakamura, T., Muto, F., Horie, T., Maekawa, S., … Molchanov, O. A. (2010). A statistical study on the correlation between lower ionospheric perturbations as seen by subionospheric VLF/LF propagation and earthquakes. *Journal of Geophysical Research*, *115*, A09305. https://doi.org/10.1029/2009JA015143

Hayakawa, M., O. A. Molchanov, & NASDA/UEC team (2004). Summary report of NASDA's earthquake remote sensing frontier project. *Physics and Chemistry of the Earth*, *29*(4-9), 617–625. https://doi.org/10.1016/j.pce.2003.08.062

He, Y., Yang, D., Qian, J., & Parrot, M. (2011). Response of the ionospheric electron density to different types of seismic events. *Natural Hazards and Earth System Sciences*, *11*(8), 2173–2180. https://doi.org/10.5194/nhess-11-2173-2011

Hobara, Y., Nakamura, R., Suzuki, M., Hayakawa, M., & Parrot, M. (2013). Ionospheric perturbations observed by the low altitude satellite DEMETER and possible relation with seismicity. *Journal of Atmospheric Electricity*, *33*(1), 21–29. https://doi.org/10.1541/jae.33.21

Hocke, K. (2008). Oscillations of global mean TEC. *Journal of Geophysical Research*, *113*, A04302. https://doi.org/10.1029/2007JA012798

Kelley, M. C., Swartz, W. E., & Heki, K. (2017). Apparent ionospheric total electron content variations prior to major earthquakes due to electric fields created by tectonic stresses. *Journal of Geophysical Research: Space Physics*, *122*, 6689–6695. https://doi.org/10.1002/2016JA023601

Kon, S., Nishihashi, M., & Hattori, K. (2011). Ionospheric anomalies possibly associated with $M \geq 6.0$ earthquakes in the Japan area during 1998-2010: Case studies and statistical study. *Journal of Asian Earth Sciences*, *41*(4-5), 410–420. https://doi.org/10.1016/j.jseaes.2010.10.005

Kuo, C. L., Huba, J. D., Joyce, G., & Lee, L. C. (2011). Ionosphere plasma bubbles and density variations induced by pre-earthquake rock currents and associated surface charges. *Journal of Geophysical Research*, *116*, A10317. https://doi.org/10.1029/2011JA016628

Li, M., & Parrot, M. (2012). "Real time analysis" of the ion density measured by the satellite DEMETER in relation with the seismic activity. *Natural Hazards and Earth System Sciences*, *12*(9), 2957–2963. https://doi.org/10.5194/nhess-12-2957-2012

Li, M., & Parrot, M. (2013). Statistical analysis of an ionospheric parameter as a base for earthquake prediction. *Journal of Geophysical Research: Space Physics*, *118*, 3731–3739. https://doi.org/10.1002/jgra.50313

Liu, J. Y., Chen, Y. I., Chen, C. H., Liu, C. Y., Chen, C. Y., Nishihashi, M., … Lin, C. H. (2009). Seismo ionospheric GPS total electron content anomalies observed before the 12 May 2008 Mw7.9 Wenchuan earthquake. *Journal of Geophysical Research*, *114*, A04320. https://doi.org/10.1029/2008JA013698

Liu, J. Y., Chuo, Y. J., Shan, S. J., Tsai, Y. B., Chen, Y. I., Pulinets, S. A., & Yu, S. B. (2004). Pre-earthquake ionospheric anomalies registered by continuous GPS TEC measurements. *Annales Geophysicae*, *22*(5), 1585–1593. https://doi.org/10.5194/%20angeo-22-1585-2004

Lühr, H., & Xiong, C. (2010). IRI-2007 model overestimates electron density during the 23/24 solar minimum. *Geophysical Research Letters*, *37*, L23101. https://doi.org/10.1029/2010GL045430

Molchanov, O. A., & Hayakawa, M. (Eds.) (2008). *Seismo electromagnetics and related phenomena: History and latest results* (189 pp.). Tokyo: TERRAPUB.

Molchanov, O. A., Hayakawa, M., Afonin, V. V., Akentieva, O. A., & Mareev, E. A. (2002). Possible influence of seismicity by gravity waves on ionospheric equatorial anomaly from data of IK-24 satellite 1, earch for idea of seismo-ionosphere coupling. In M. Hayakawa & O. A. Molchanov (Eds.), *Seismo electromagnetics (Lithosphere-Atmosphere-Ionosphere Coupling)* (pp. 275–285). Tokyo, Japan: TERRAPUB.

Němec, F., Santolík, O., & Parrot, M. (2009). Decrease of intensity of ELF/VLF waves observed in the upper ionosphere close to earthquakes: A statistical study. *Journal of Geophysical Research*, *114*, A04303. https://doi.org/10.1029/2008JA013972

Němec, F., Santolík, O., Parrot, M., & Berthelier, J. J. (2008). Spacecraft observations of electromagnetic perturbations connected with seismic activity. *Geophysical Research Letters*, *35*, L05109. https://doi.org/10.1029/2007GL032517

Omori, Y., Yasuoka, Y., Nagahama, H., Kawada, Y., Ishikawa, T., Tokonami, S., & Shinogi, M. (2007). Anomalous radon emanation linked to preseismic electromagnetic phenomena. *Natural Hazards and Earth System Sciences*, *7*(5), 629–635. https://doi.org/10.5194/nhess-7-629-2007

Ouzounov, D., Liu, D., Chunli, K., Cervone, G., Kafatos, M., & Taylor, P. (2007). Outgoing long wave radiation variability from IR satellite data prior to major earthquakes. *Tectonophysics*, *431*(1–4), 211–220. https://doi.org/10.1016/j.tecto.2006.05.042

Ouzounov, D., Pulinets, S., Romanov, A., Romanov, A., Tsybulya, K., Davidenko, D., … Taylor, P. (2011). Atmosphere-ionosphere response to the M9 Tohoku earthquake revealed by multi-instrument space-borne and ground observations: Preliminary results. *Earthquake Science*, *24*(6), 557–564. https://doi.org/10.1007/s11589-011-0817-z

Parrot, M. (Ed.) (2006). Special issue: First results of the DEMETER micro-satellite. *Planetary and Space Science*, *54*(5), 411–412. https://doi.org/10.1016/j.pss.2005.10.012

Parrot, M. (2011). Statistical analysis of the ion density measured by the satellite DEMETER in relation with the seismic activity. *Earthquake Science*, *24*(6), 513–521. https://doi.org/10.1007/s11589-011-0813-3

Parrot, M. (2012). Statistical analysis of automatically detected ion density variations recorded by DEMETER and their relation to seismic activity. *Annales Geophysicae*, *55*(1), 149–155. https://doi.org/10.4401/ag-5270

Píša, D., Němec, F., Parrot, M., & Santolík, O. (2012). Attenuation of electromagnetic waves at the frequency ~1.7 kHz in the vicinity of earthquakes observed in the upper ionosphere by the DEMETER satellite. *Annales Geophysicae*, *55*(1), 157–163. https://doi.org/10.4401/ag-5276

Píša, D., Němec, F., Santolík, O., Parrot, M., & Rycroft, M. (2013). Additional attenuation of natural VLF electromagnetic waves observed by the DEMETER spacecraft resulting from pre-seismic activity. *Journal of Geophysical Research: Space Physics*, *118*, 5286–5295. https://doi.org/10.1002/jgra.50469

Pulinets, S. A. (2007). Natural radioactivity, earthquakes, and the ionosphere. *Eos, Transactions American Geophysical Union*, *88*(20), 217–218. https://doi.org/10.1029/2007EO200001

Pulinets, S. A. (2009). Lithosphere-Atmosphere-Ionosphere Coupling (LAIC) model. In M. Hayakawa (Ed.), *Electromagnetic phenomena associated with earthquakes* (pp. 235–253). Kerala, India: Transworld Research Network.

Pulinets, S. A. (2012). Low-latitude atmosphere-ionosphere effects initiated by strong earthquakes preparation process. *International Journal of Geophysics*, *2012*, 131842. https://doi.org/10.1155/2012/131842

Pulinets, S. A., & Ouzounov, D. (2011). Lithosphere-Atmosphere-Ionosphere Coupling (LAIC) model: An unified concept for earthquake precursors validation. *Journal of Asian Earth Sciences*, *41*(4-5), 371–382. https://doi.org/10.1016/j.jseaes.2010.03.005

Pulinets, S. A., Ouzounov, D. P., Karelin, A. V., & Davidenko, D. V. (2015). Physical bases of the generation of short-term earthquake precursors: A complex model of ionization-induced geophysical processes in the lithosphere-atmosphere-ionosphere-magnetosphere system. *Geomagnetism and Aeronomy*, *55*(4), 521–538. https://doi.org/10.1134/S0016793215040131

Rolland, L. M., Lognonné, P., Astafyeva, E., Kherani, E. A., Kobayashi, N., Mann, M., & Munekane, H. (2011). The resonant response of the ionosphere imaged after the 2011 off the Pacific coast of Tohoku earthquake. *Earth, Planets and Space*, *63*(7), 853–857. https://doi.org/10.5047/eps.2011.06.020

Ryu, K., Lee, E., Chae, J. S., Parrot, M., & Pulinets, S. (2014). Seismo-ionospheric coupling appearing as equatorial electron density enhancements observed via DEMETER electron density measurements. *Journal of Geophysical Research: Space Physics*, *119*, 8524–8542. https://doi.org/10.1002/2014JA020284

Sorokin, V. M. (2007). Plasma and electromagnetic effects in the ionosphere related to the dynamics of charged aerosols in the lower atmosphere. *Russian Journal of Physical Chemistry B*, *1*(2), 138–170. https://doi.org/10.1134/%20S199079310702008X

Sorokin, V. M., Chmyrev, V. M., & Hayakawa, M. (Eds.) (2015). *Electrodynamic coupling of lithosphere-atmosphere-ionosphere of the Earth* (326 pp.). Hauppauge, New York: Nova Science Publishers.